buildings

MDPI

Article

Correlation Analysis Between Structural Seismic Response and Ground Motion Parameters Considering SSI Effects

Bowen Zheng, Peizhen Li and Jinping Yang *

State Key Laboratory of Disaster Reduction in Civil Engineering, Tongji University, Shanghai 200092, China
* Correspondence: jping_yang@haut.edu.cn

Abstract

Investigating the relationship between ground motion intensity measures (IMs) and structural responses is fundamental to seismic hazard assessment and performance-based structural design. However, most existing studies are based on the fixed-base assumption, where foundation flexibility is neglected, limiting the understanding of the effects of Soil–Structure Interaction (SSI) on IM–engineering demand parameters (EDPs) correlations. This study systematically evaluates the correlations between various IMs and EDPs while explicitly accounting for SSI effects, with particular emphasis on the influence of ground motion type (near-fault and far-field records). The results indicate that SSI modifies the correlations between IMs and structural responses, although its influence varies among different categories of IMs. For acceleration-based IMs, SSI has a limited impact on their relative effectiveness, preserving their ranking despite moderate changes in correlation coefficients. Velocity-based IMs consistently exhibit the strongest correlations with structural responses; however, their relative performance is strongly dependent on the characteristics of the input ground motions. In contrast, displacement-based IMs demonstrate substantial sensitivity to both soil conditions and ground motion characteristics, resulting in pronounced variability in their predictive capability across different seismic scenarios. These findings highlight the important influence of SSI in IM–EDP correlation analysis and emphasize the necessity of incorporating foundation flexibility when selecting candidate IMs for seismic performance assessment. The results are expected to improve the understanding of IM–response correlations in SSI systems and may help inform the preliminary screening of candidate IMs for performance-based earthquake engineering applications.

Keywords: soil–structure interaction; seismic intensity measures; correlation analysis; ground motion selection; seismic response

Check for updates

Academic Editor: Antonio Formisano

Received: 28 May 2026
Revised: 23 June 2026
Accepted: 24 June 2026
Published: 27 June 2026

Copyright: © 2026 by the authors. Licensee MDPI, Basel, Switzerland. This article is an open access article distributed under the terms and conditions of the Creative Commons Attribution (CC BY) license.

1. Introduction

In earthquake engineering, rigorous assessment of structural seismic performance is of critical importance. The seismic response of a structure is influenced not only by its inherent dynamic characteristics but also by the characteristics of the input ground motion. Conventional dynamic time-history analysis, which simulates structural responses by solving equations of motion, is computationally intensive and provides limited insight into generalized response trends. Therefore, investigating statistical correlations between key IMs, such as peak acceleration, velocity, and spectral characteristics, and structural demand parameters, such as maximum displacement and inter-story drift ratio, has emerged as an effective approach. This methodology shifts the focus from tracking complete response his-

tories to establishing statistical predictive relationships, thereby substantially streamlining performance-based earthquake engineering (PBEE) frameworks.

To this end, numerous researchers have proposed and evaluated advanced IMs to better characterize seismic damage potential. For instance, building upon the pseudo-acceleration spectrum shape parameter Np, Bojórquez et al. [1] proposed a novel seismic intensity measure (IB), which effectively accounts for structural nonlinearity and higher-mode effects in steel frames. Similarly, Chen et al. [2] developed an energy-frequency-based IM derived from the Hilbert–Huang Transform (HHT), demonstrating a strong period-independent linear correlation with structural responses. Other studies have focused on specific structural systems. Hui et al. [3] established that the PGV/PGA ratio serves as an effective predictor of pile foundation responses in liquefied soils, while Kamal et al. [4] and Chen et al. [5] demonstrated that velocity-related parameters generally outperform acceleration- and displacement-based parameters in predicting the responses of underground tunnels and multi-story buildings, respectively. Furthermore, comprehensive analyses conducted by Chebihi [6] and Li [7] highlighted that the optimal IM is inherently dependent on both the selected engineering demand parameter (e.g., base shear versus drift) and the structural configuration. The application of IM correlation analysis has also significantly advanced the development of structural fragility curves and collapse assessment. Studies by Seyedi et al. [8] and Singh et al. [9] demonstrated that employing multiple IMs, or vector-based IMs that simultaneously capture structural and ground motion characteristics, can substantially reduce dispersion in fragility surfaces. For highly nonlinear limit states such as structural collapse, Shi et al. [10] identified the mean period (T_m), significant duration (D_s), and PGA as the most effective predictors of seismic responses of base-isolated structures. Advanced predictive models, such as the multivariate regression formulations by Durucan et al. [11] and the artificial neural network (ANN) frameworks developed by Wani et al. [12], have further improved the efficiency and sufficiency of IMs for specific structural typologies.

Specialized seismic scenarios, particularly near-fault ground motions, require careful selection of IMs due to their distinct energy characteristics. Researchers such as Mollaioli et al. [13] and Yang et al. [14] have extensively explored the predictive capabilities of various IMs under near-fault ground motions with and without velocity pulses. Their findings consistently highlight the importance of velocity- and displacement-related parameters, such as improved effective peak velocity (IEPV), in predicting the responses of medium- to long-period structures. Furthermore, Wei et al. [15] and Wang et al. [16] demonstrated that pulse-like ground motions exert significant influences on the seismic behavior of complex coupled systems, including high-speed railway bridges, indicating that optimal IMs selection should account for the frequency characteristics of the seismic hazard. Beyond structural engineering applications, IM–response correlation analyses have also been widely applied in geotechnical engineering, contributing to levee performance assessment [17], seismic slope stability [18], and rapid regional macroseismic intensity prediction [19]. In addition, robust IM–response correlation relationships provide an important benchmark for validating artificial ground motion generation methods, ensuring that simulated records possess damage potential comparable to that of natural earthquake records [20,21].

Despite these significant advancements, an important limitation remains in the existing literature: the vast majority of IM correlation studies are conducted under the fixed-base assumption. Recent investigations have shown that SSI can significantly influence key seismic demand parameters, such as inter-story drift ratio and base shear, in soil–foundation–structure systems, indicating that fixed-base models may not adequately capture the actual seismic behavior of structures founded on deformable soils [22]. In

practice, seismic excitation induces complex interactions between the soil medium, foundation, and superstructure. Soil nonlinearity, foundation flexibility, and degradation of dynamic stiffness [23] can modify both the characteristics of the transmitted ground motion and the dynamic properties of the structural system [24], resulting in phenomena such as period elongation and increased damping. Recent studies on structural health monitoring and operational modal identification further indicate that modal parameters, such as natural frequencies and damping ratios, can be affected by environmental conditions, operational states, and boundary uncertainties. For example, stochastic subspace identification and ambient vibration-based techniques have been used to track variations in dynamic parameters from measured structural responses, while temperature changes and support-condition fluctuations may alter the identified fundamental frequencies of benchmark structures. In addition, high-fidelity finite element models can provide detailed representations of local stress states, boundary conditions, and material nonlinearities under earthquake excitation [25]. These studies provide useful methodological context for the present work, although this study adopts a macro-scale Bouc–Wen hysteretic model and a lumped-parameter SSI model to efficiently conduct correlation analyses over a large suite of ground motion records and soil conditions. Moreover, the soil medium acts as a dynamic filter, altering the frequency content of seismic waves and introducing additional translational and rotational foundation motions. These effects can substantially influence the seismic response of structures, particularly for high-rise buildings, long-span bridges, and structures founded on soft soils. Consequently, neglecting SSI effects may lead to biased estimations of structural demand and limit the applicability of IM–response correlation relationships established using fixed-base models. Although considerable efforts have been devoted to identifying optimal IMs for different structural systems and seismic scenarios, the influence of SSI on IM–response correlation remains insufficiently understood. This knowledge gap motivates the need for a systematic investigation of IM–response correlations considering SSI effects.

Therefore, this study aims to systematically investigate the correlation between IMs and structural responses while explicitly accounting for SSI effects. By developing a coupled lumped-parameter soil–structure system model, the study seeks to clarify how SSI influences the relationships between key IMs and structural demand parameters, with particular emphasis on the differences between far-field and near-fault ground motions. The results are expected to improve the understanding of IM–response correlations in SSI systems and contribute to more realistic assessments of seismic structural performance. Furthermore, the findings may be expected to improve the understanding of IM–response correlations in SSI systems and to inform the preliminary selection of candidate IMs for performance-based earthquake engineering applications.

2. Methodology

This section describes the numerical analysis framework developed to investigate the correlations between IMs and EDP while explicitly accounting for SSI effects. The framework consists of two main components: (i) the development of a coupled soil–foundation–structure numerical model, and (ii) the selection of a comprehensive suite of seismic IMs for subsequent statistical analyses.

2.1. Research Significance

Quantifying these correlations is of fundamental importance for two primary reasons. First, it enhances predictive capability by enabling the estimation of structural response characteristics from selected IMs. From a methodological perspective, this process can be regarded as a form of feature preselection, whereby informative relationships between input

ground motion characteristics and structural responses are identified prior to predictive modeling. Second, it facilitates the selection of representative ground motions from large databases that satisfy predefined structural performance objectives, thereby providing a rational basis for performance-based seismic design. Figure 1 schematically illustrates the significance of this correlation analysis.

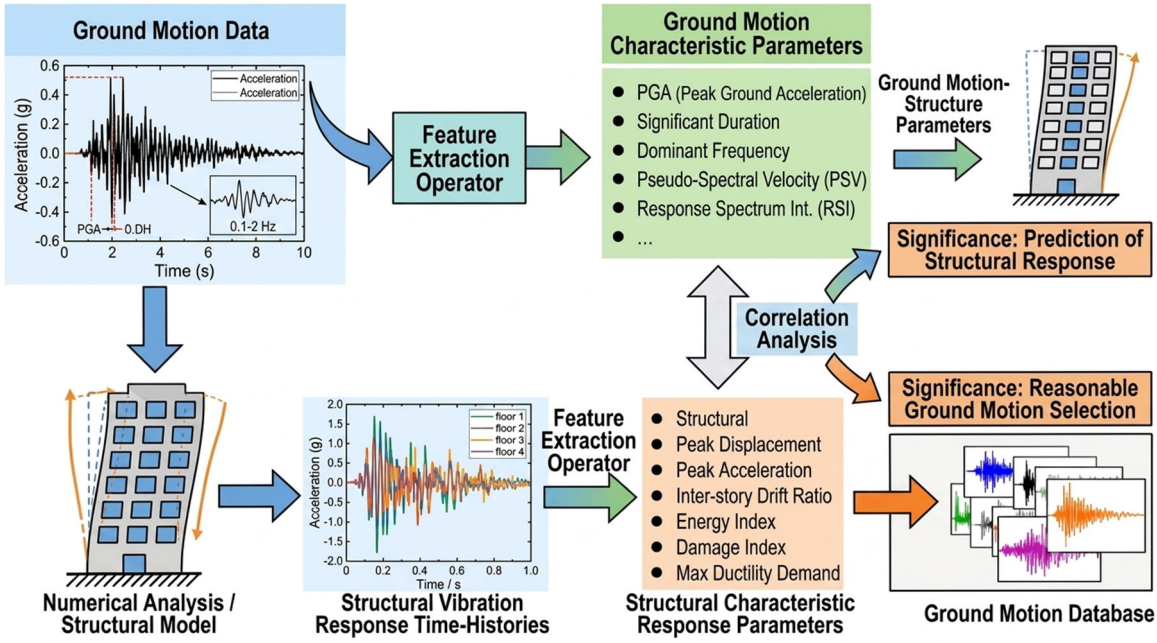


Figure 1. Schematic representation of the correlation between ground motion parameters and structural responses.

2.2. Coupled Soil–Structure System Modeling

To efficiently and accurately simulate the dynamic interaction between the superstructure and the underlying soil, this study adopts a lumped-parameter approach for SSI. The method represents the flexibility and energy dissipation of the soil half-space by an equivalent system comprising springs, dashpots, and a lumped mass attached to the structural foundation. This approach achieves a reasonable balance between computational efficiency and physical fidelity, making it highly suitable for parametric studies.

2.2.1. Superstructure Model

The superstructure is idealized as an n-degree-of-freedom (MDOF) planar shear-beam model. Its dynamic properties are defined by a lumped mass matrix, a lateral stiffness matrix, and a Rayleigh damping matrix, as depicted in the schematic diagram of the fixed-base computational model (Figure 2).

To account for structural nonlinearity, the inter-story restoring force is modeled using the generalized Bouc–Wen model [26]. The restoring force is expressed as a combination of linear elastic and hysteretic components, formulated as a function of the inter-story relative displacement u and a hysteretic displacement variable z:

$$f_s(u,z) = \alpha k u + (1-\alpha)kz \tag{1}$$

The global equation of motion for the MDOF structure subjected to seismic excitation can be written as:

$$M\ddot{x} + C\dot{x} + K_e x + K_h z = -MI\ddot{x}_g \tag{2}$$

where M and C denote the mass and damping matrices of the superstructure, respectively. $\mathbf{x}$ is the displacement vector relative to the base. I is the influence vector, and $\ddot{x}_g$ is the input ground acceleration. The elastic stiffness matrix K_e and the hysteretic stiffness matrix K_h are assembled as follows:

$$K_e = \begin{bmatrix} \alpha_1 k_1 & -\alpha_2 k_2 & & \cdots & & 0 \\ & \alpha_2 k_2 & -\alpha_3 k_3 & & & \\ & \vdots & & \ddots & & \\ & & & \cdots & \alpha_{n-1} k_{n-1} & -\alpha_n k_n \\ 0 & & & & & \alpha_n k_n \end{bmatrix} \tag{3}$$

$$K_h = \begin{bmatrix} (1-\alpha_1)k_1 & -(1-\alpha_2)k_2 & & & & 0 \\ & (1-\alpha_2)k_2 & -(1-\alpha_3)k_3 & & & \\ & & & \ddots & & \\ & & & \cdots & (1-\alpha_{n-1})k_{n-1} & -(1-\alpha_n)k_n \\ 0 & & & & & (1-\alpha_n)k_n \end{bmatrix} \tag{4}$$

The evolution of the hysteretic variable z is governed by the following nonlinear differential equations:

$$\dot{Z} = h(Z)\frac{A_{bw}\dot{U} - v\left(\beta_{BW}\left|\dot{U}\right||Z|^{n_{BW}-1}Z + \gamma_{BW}\dot{U}|Z|^{n_{BW}}\right)}{\eta} \tag{5}$$

$$v = 1 + \delta_{v_{BW}}\varepsilon \tag{6}$$

$$\eta = 1 + \delta_{\eta_{BW}}\varepsilon \tag{7}$$

$$\varepsilon(t) = \int_0^t Z\dot{U}dt \tag{8}$$

$$h(Z) = 1 - \xi_1 exp\left[-\frac{Zsgn\left(\dot{U}\right) - q_{BW}Z_u}{\xi_2}\right]^2 \tag{9}$$

$$\xi_1(\varepsilon) = \xi_{s_{BW}}\left(1 - e^{-p_{BW}\varepsilon}\right) \tag{10}$$

$$\xi_2(\varepsilon) = \left(\psi_{BW} + \delta_{\psi_{BW}}\varepsilon\right)\left(\lambda_{BW} + \xi_1(\varepsilon)\right) \tag{11}$$

$$Z_u = \left(\frac{A_{BW}}{v(\beta_{BW} + \gamma_{BW})}\right)^{1/n_{BW}} \tag{12}$$

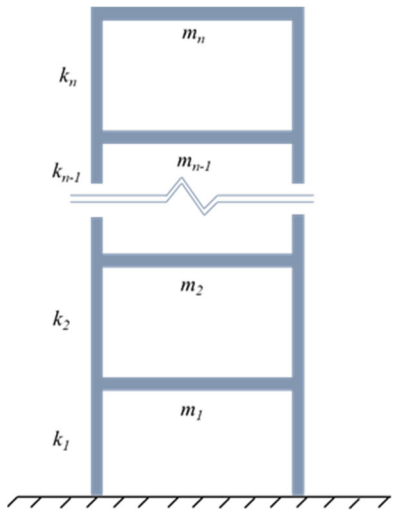


Figure 2. Schematic of the fixed-base structural model.

2.2.2. Soil–Structure Interaction Modeling

For the structural system incorporating SSI effects, the translational displacement x_0 and rocking rotation θ_0 of the foundation are introduced as additional degrees of freedom (DOFs) in addition to those of the superstructure [26,27]. Figure 3 illustrates the structural model incorporating SSI effects. Accordingly, the global mass [M], damping [C], and stiffness [K] matrices of the interactive system are augmented as follows:

$$[M] = \begin{bmatrix} [M_f] & [M_v] & [MH] \\ [M_v]^T & m_0 + \left(\sum_{i=1}^{N} m_i\right) & \left(\sum_{i=1}^{N} m_i h_i\right) \\ [MH]^T & \left(\sum_{i=1}^{N} m_i h_i\right) & \left(\sum_{i=1}^{N} m_i h_i^2\right) + I_0 + \sum_{i=1}^{N} I_i \end{bmatrix} \tag{13}$$

$$[M_v] = [m_1,\ m_2, \ldots, m_{N-1},\ m_N]^T \tag{14}$$

$$[MH] = [m_1 h_1,\ m_2 h_2,\ \cdots, m_{N-1} h_{N-1},\ m_N h_N]^T \tag{15}$$

$$[C] = \begin{bmatrix} [C_f] & 0 & 0 \\ 0 \ldots 0 & c_s & 0 \\ 0 \ldots 0 & 0 & c_r \end{bmatrix} \tag{16}$$

$$[C_f] = \begin{bmatrix} (c_1 + c_2) & -c_2 & 0 & \cdots & 0 \\ -c_2 & (c_2 + c_3) & -c_3 & & \\ \vdots & & & \ddots & \vdots \\ 0 & & & \cdots & \begin{matrix} c_{N-1} + c_N & -c_N \\ -c_N & c_N \end{matrix} \end{bmatrix} \tag{17}$$

$$[K] = \begin{bmatrix} [K_f] & 0 & 0 \\ 0 \ldots 0 & k_s & 0 \\ 0 \ldots 0 & 0 & k_r \end{bmatrix} \tag{18}$$

$$[K_f] = \begin{bmatrix} (k_1 + k_2) & -k_2 & 0 & \cdots & 0 \\ -k_2 & (k_2 + k_3) & -k_3 & & \\ \vdots & & & \ddots & \vdots \\ 0 & & & \cdots & \begin{matrix} k_{N-1} + k_N & -k_N \\ -k_N & k_N \end{matrix} \end{bmatrix} \tag{19}$$

$$[m^*] = \begin{bmatrix} m_1 \\ m_2 \\ \vdots \\ m_{N-1} \\ m_N \\ m_0 + \left(\sum_{i=1}^{N} m_i\right) \\ \left(\sum_{i=1}^{N} m_i h_i\right) \end{bmatrix} \tag{20}$$

$$\{x(t)\} = [x_1, x_2, \cdots, x_{N-1}, x_N, x_0, \theta_0]^T \tag{21}$$

In this study, to isolate the influence of foundation flexibility, nonlinear behavior is confined to the superstructure and modeled using the Bouc–Wen model. The soil medium and the foundation are assumed to remain linearly elastic throughout seismic excitation. It should be noted that the adopted lumped-parameter SSI model does not explicitly account for nonlinear soil behavior, such as strain-dependent stiffness degradation, damping increase, plastic deformation, and foundation-related nonlinearities. This simplification is adopted to maintain a consistent and computationally efficient framework for investigating the influence of foundation flexibility on IM–EDP correlation patterns over a large suite of ground motion records. Under strong ground motions, particularly near-fault records and soft-soil conditions, nonlinear soil behavior may further modify the effective stiffness and damping of the soil–foundation system and consequently influence the predicted structural responses and IM–EDP correlations. Therefore, the results of this study should be interpreted as correlation trends for linear-elastic lumped-parameter SSI systems. Future studies may incorporate equivalent-linear or fully nonlinear soil models to further examine the influence of soil nonlinearity.

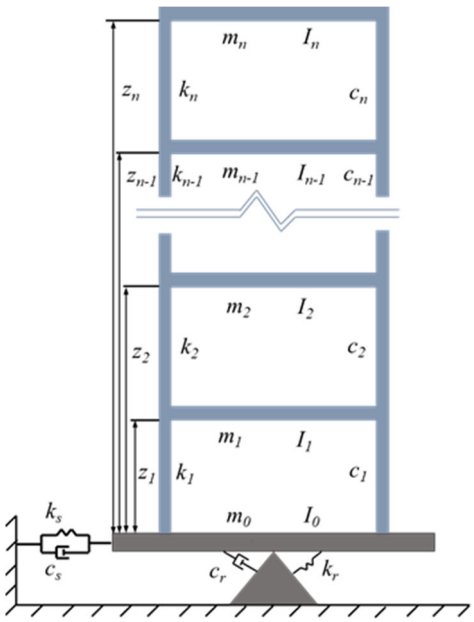


Figure 3. Schematic of the structural model considering SSI effects.

2.3. Ground Motion Intensity Measures (IMs)

To systematically evaluate the correlations between various IMs and structural responses, a comprehensive set of seismic IMs was selected based on a review of the existing literature. These IMs are broadly categorized into acceleration-based, velocity-based, and

displacement-based groups. Their definitions and corresponding mathematical expressions are summarized in Table 1.

Table 1. Definitions of the selected ground motion intensity measures.

Acceleration Type		Velocity Type		Displacement Type	
PGA	$\max\left\|\ddot{u}_g(t)\right\|$	PGV	$\max\left\|\dot{u}_g(t)\right\|$	PGD	$\max\left\|u_g(t)\right\|$
a_{sq}	$\int_0^{T_f}\left[\ddot{u}_g(t)\right]^2 dt$	v_{sq}	$\int_0^{T_f}\left[\dot{u}_g(t)\right]^2 dt$	d_{sq}	$\int_0^{T_f}\left[u_g(t)\right]^2 dt$
a_{rs}	$\sqrt{\int_0^{T_f}\left[\ddot{u}_g(t)\right]^2 dt}$	v_{rs}	$\sqrt{\int_0^{T_f}\left[\dot{u}_g(t)\right]^2 dt}$	d_{rs}	$\sqrt{\int_0^{T_f}\left[u_g(t)\right]^2 dt}$
P_a	$\frac{\int_{t_5}^{t_{95}}\left[\ddot{u}_g(t)\right]^2 dt}{t_{95}-t_5}$	P_v	$\frac{\int_{t_5}^{t_{95}}\left[\dot{u}_g(t)\right]^2 dt}{t_{95}-t_5}$	P_d	$\frac{\int_{t_5}^{t_{95}}\left[u_g(t)\right]^2 dt}{t_{95}-t_5}$
a_{rms}	$\sqrt{P_a}$	v_{rms}	$\sqrt{P_v}$	d_{rms}	$\sqrt{P_d}$
I_a	$PGA \cdot T_D^{1/3}$	I_v	$PGV^{2/3} \cdot T_D^{1/3}$	I_d	$PGD \cdot T_D^{1/3}$
I_c	$a_{rms}^{1.5} \cdot T_D^{0.5}$	I_F	$PGV \cdot T_D^{0.25}$		
I_A	$\frac{\pi}{2g}\int_0^{T_f}\left[\ddot{u}_g(t)\right]^2 dt$	SI	$\int_{0.1}^{2.5} S_v(T,\xi=0.05)dT$		
		P_D	I_A/v_0^2		

3. Numerical Modeling and Result Analysis

This section presents a numerical case study that investigates the correlations between IMs and the maximum inter-story drift ratio (MIDR) of a structure, while explicitly accounting for SSI effects. To capture potential differences in correlation patterns, the analysis explicitly evaluates the influence of ground motion types, distinguishing between near-fault and far-field records.

All nonlinear dynamic analyses were conducted using an in-house Python code (version 3.11.7). The coupled equations of motion of the fixed-base and SSI systems were solved using the classical fourth-order Runge–Kutta method with a fixed integration time step of 0.02 s. The selected records were processed using a consistent time-step format before response of history analysis. The maximum inter-story drift ratio was extracted from the computed displacement response histories for each ground motion record.

To ensure consistency in the statistical analysis, all IMs and MIDR values were extracted using a unified post-processing procedure, and the record identifiers, model cases, units, and response quantities were checked before calculating the Pearson correlation coefficients. MIDR is defined as the maximum absolute inter-story drift ratio over all stories and over the entire duration of each ground motion record. Specifically, MIDR is calculated as:

$$MIDR = \max_{i,t}\left|\frac{\Delta_i(t)}{h_i}\right| \tag{22}$$

where h_i is the story height and $\Delta_i(t)$ is the relative horizontal displacement between two adjacent floors $\Delta_i(t) = u_i(t) - u_{i-1}(t)$. For the fixed-base model, the relative displacement for the first story is equal to the absolute horizontal displacement of the first floor (since the base displacement is zero), and for the other stories, it is equal to the relative displacement between the current floor and the one immediately below it. For the SSI model, the foundation translation and rocking are introduced as additional degrees of freedom. Since the rigid foundation translation is common to all floors, it cancels out in the inter-story relative displacement, while the contribution of foundation rocking is included as $h_i\theta_0(t)$. Therefore, the inter-story displacement in the SSI model is calculated as $\Delta_i(t) = u_i(t) - u_{i-1}(t) + h_i\theta_0(t)$. MIDR is then obtained as $\max_{i,t}\left|\frac{\Delta_i(t)}{h_i}\right|$.

The correlations between IMs and MIDR are quantified using the Pearson correlation coefficient, as defined in Equation (23).

$$\rho_{X,Y} = \frac{Cov(X,Y)}{\sigma_X \sigma_Y} = \frac{E[(X-\mu_X)(Y-\mu_Y)]}{\sigma_X \sigma_Y} \tag{23}$$

where $\rho_{X,Y}$ is the Pearson correlation coefficient between X and Y; $Cov(X,Y)$ denotes the covariance between X and Y; μ_X and μ_Y are the mean values of X and Y; and $E[\cdot]$ represents the expectation operator;

The coefficient $\boldsymbol{\rho_{X,Y}}$ takes values in the range $[-1, 1]$, where values close to 1 or -1 indicate strong linear correlation, and values near 0 indicate weak or no linear correlation.

3.1. Description of Prototype Structure

The prototype structure is a 40-story building, with a first-story height of 3.6 m and a typical height of 3.0 m for all upper stories. The lateral story stiffness decreases gradually from 21.3×10^8 N/m at the base to 9.8×10^8 N/m at the top, while the mass of each story is constant at 9.8×10^5 kg. The mass moment of inertia of each story is 1.31×108 kg·m^2. The foundation is modeled with a radius of 20 m, a mass of 1.96×10^6 kg, and a mass moment of inertia of 1.96×108 kg·m^2. Rayleigh damping is adopted for the structural model. The parameters of the generalized Bouc–Wen model are detailed in Table 2 [26,28]. To evaluate the impact of SSI, the correlation between IMs and structural responses is investigated under various foundation soil conditions. The equivalent lumped spring and dashpot parameters for the respective soil categories are summarized in Table 3 [27].

Table 2. Parameters of the generalized Bouc–Wen model.

	α_{BW}	A_{BW}	n_{BW}	β_{BW}	γ_{BW}	$\delta_{v_{BW}}$	$\delta_{\eta_{BW}}$	p_{BW}	q_{BW}	ψ_{BW}	$\delta_{\psi_{BW}}$	λ_{BW}	$\xi_{s_{BW}}$
Value	0.44	1	1	320	150	2000	2000	1000	0.25	0.05	5	0.5	0.99

Table 3. Equivalent dynamic parameters for various soil conditions.

Soil Type	Translational Stiffness k_s (N/m)	Rotational Stiffness k_r (N·m)	Translational Damping c_s (N·s/m)	Rotational Damping c_r (N·s·m)
Soft	1.91×10^9	7.53×10^{11}	2.19×10^8	2.26×10^{10}
Neutral	1.80×10^{10}	7.02×10^{12}	6.90×10^8	7.02×10^{10}
Dense	5.75×10^{10}	1.91×10^{13}	1.32×10^9	1.15×10^{11}

3.2. Selection of Ground Motion Records

Following the recommendations of FEMA P695 and the ATC-63 report [29], this study selects a ground motion suite consisting of 41 far-field (FF) and 55 near-fault (NF) records for nonlinear dynamic analysis. The selection criteria include a moment magnitude M > 6.5, Joyner–Boore distances R_{JB} > 10 (FF) and R_{JB} < 10 km (NF), and NEHRP site classes C and D. No amplitude scaling was applied to the selected ground motion records. All nonlinear dynamic analyses were performed using the as-recorded acceleration time histories. This treatment was adopted because the objective of this study is to investigate the record-to-record correlation between ground motion intensity measures and engineering demand parameters, rather than to assess structural responses at a prescribed hazard level. Using unscaled records preserves the natural variability of earthquake intensity, frequency content, duration, and near-fault/far-field characteristics, which is essential for evaluating the statistical relationship between IMs and EDPs. Therefore, the response spectra shown

in Figure 4 correspond to the original unscaled ground motion records. Figure 4 presents the acceleration response spectra of the selected ground motion records.

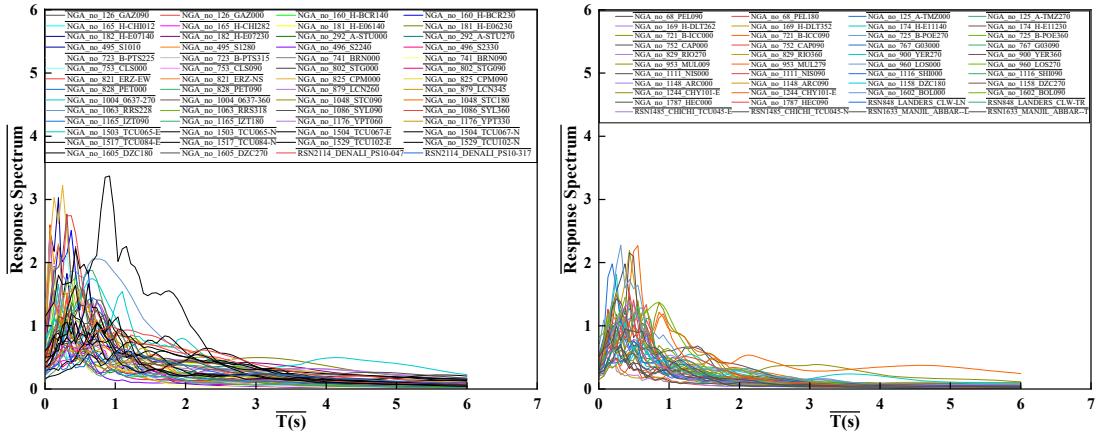


Figure 4. Acceleration response spectra of different types of ground motion sets.

3.3. Correlation Analysis Between MIDR and IMs

3.3.1. Acceleration-Based Intensity Measures

Figure 5 presents scatter plots of acceleration-based IMs against MIDR for the four structural models under far-field ground motions. The Pearson correlation coefficient, R, is shown in each subplot. Under far-field motions, the ranking of correlations between acceleration-based IMs and MIDR remains consistent across all models as: I_a, a_{rs}, $a_{sq}(I_a)$, PGA, I_c, a_{rms}, and P_a. This indicates that SSI has negligible influence on the relative ranking of acceleration-based IM effectiveness, although it modifies the structural response amplitude and period.

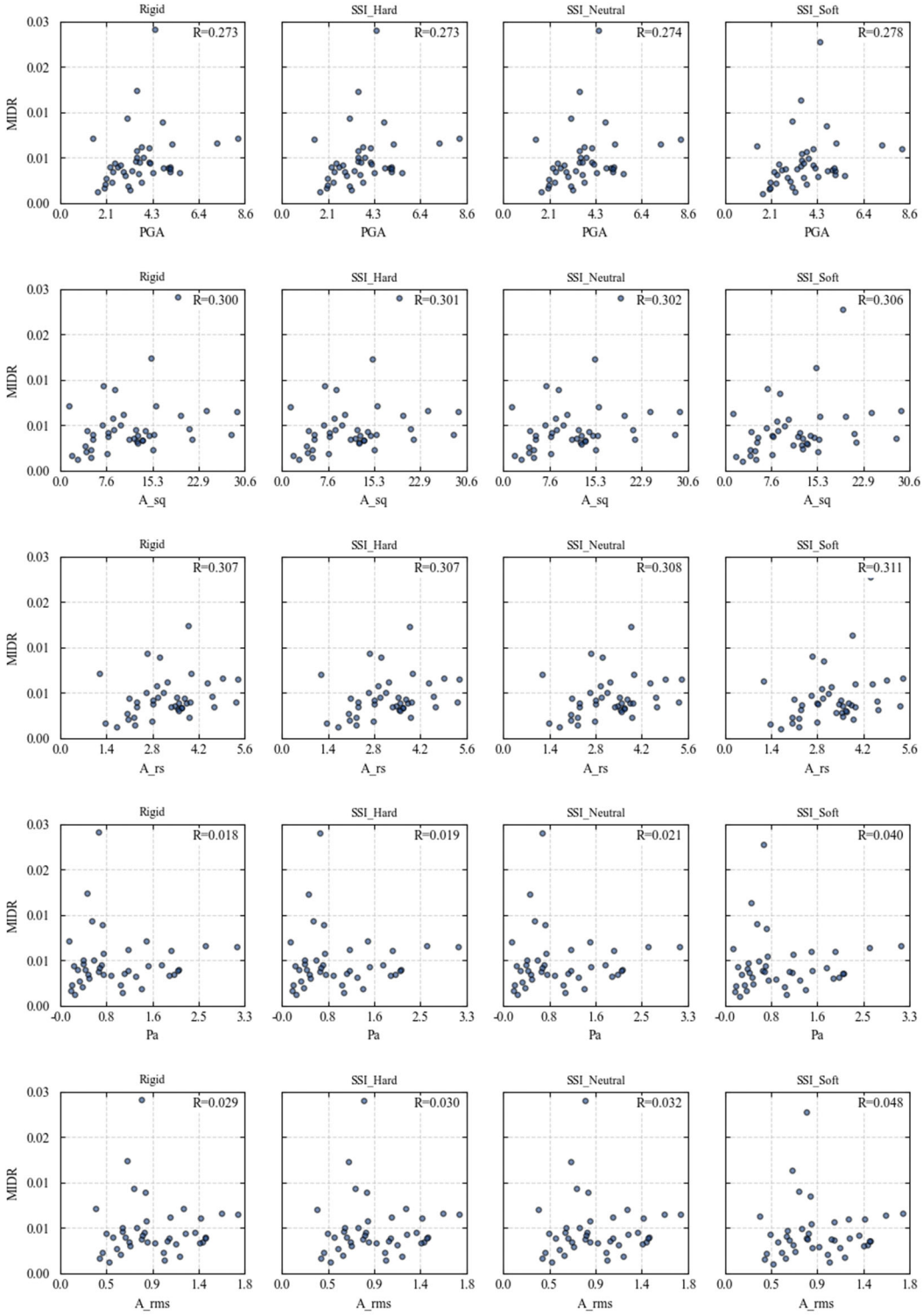


Figure 5. *Cont*.

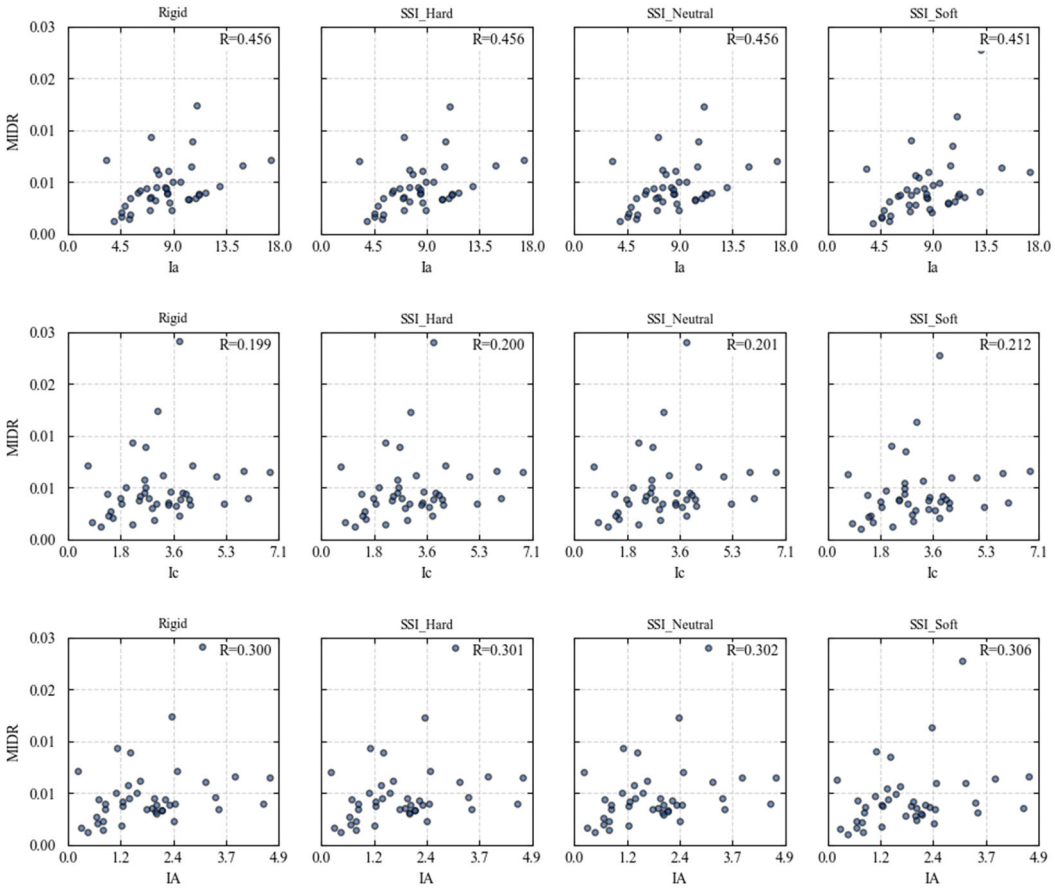


Figure 5. Scatter plots of acceleration-based IMs against MIDR under far-field ground motions.

However, the absolute correlations remain generally low. This is primarily attributed to the long-period characteristics of the studied high-rise structure (fixed-base period = 3.83 s), which becomes more pronounced under SSI-induced period elongation. In this range, structural response is dominated by velocity and displacement components rather than acceleration, leading to weak correlation with acceleration-based IMs such as PGA.

Figure 6 presents scatter plots of acceleration-based IMs against MIDR under near-fault ground motions. The correlation ranking shifts to: a_{rs}, $a_{sq}(I_a)$, I_c, a_{rms}, P_a, I_a, and PGA. Similar to the far-field case, SSI does not significantly alter the ranking of correlation magnitudes. Compared with far-field motions, near-fault records exhibit reduced correlations for PGA, which also weakens the correlation of Ia. In contrast, energy-related IMs (e.g., a_{rs} and $a_{sq}(I_a)$) exhibit the highest correlations with structural responses due to their ability to capture the concentrated energy and pulse characteristics of near-fault ground motions. Averaged parameters such as *Pa* and arms also show improved performance under near-fault conditions.

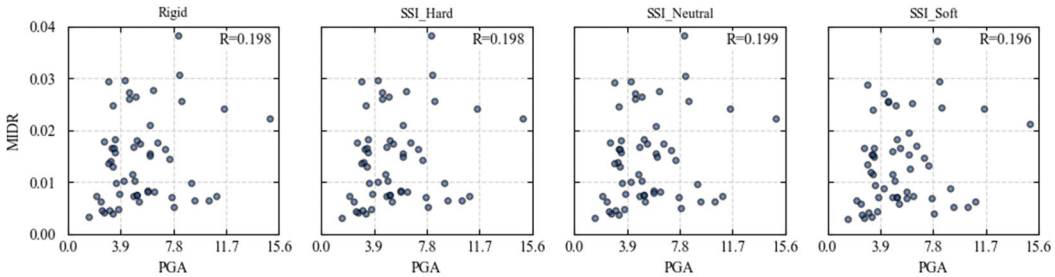


Figure 6. *Cont.*

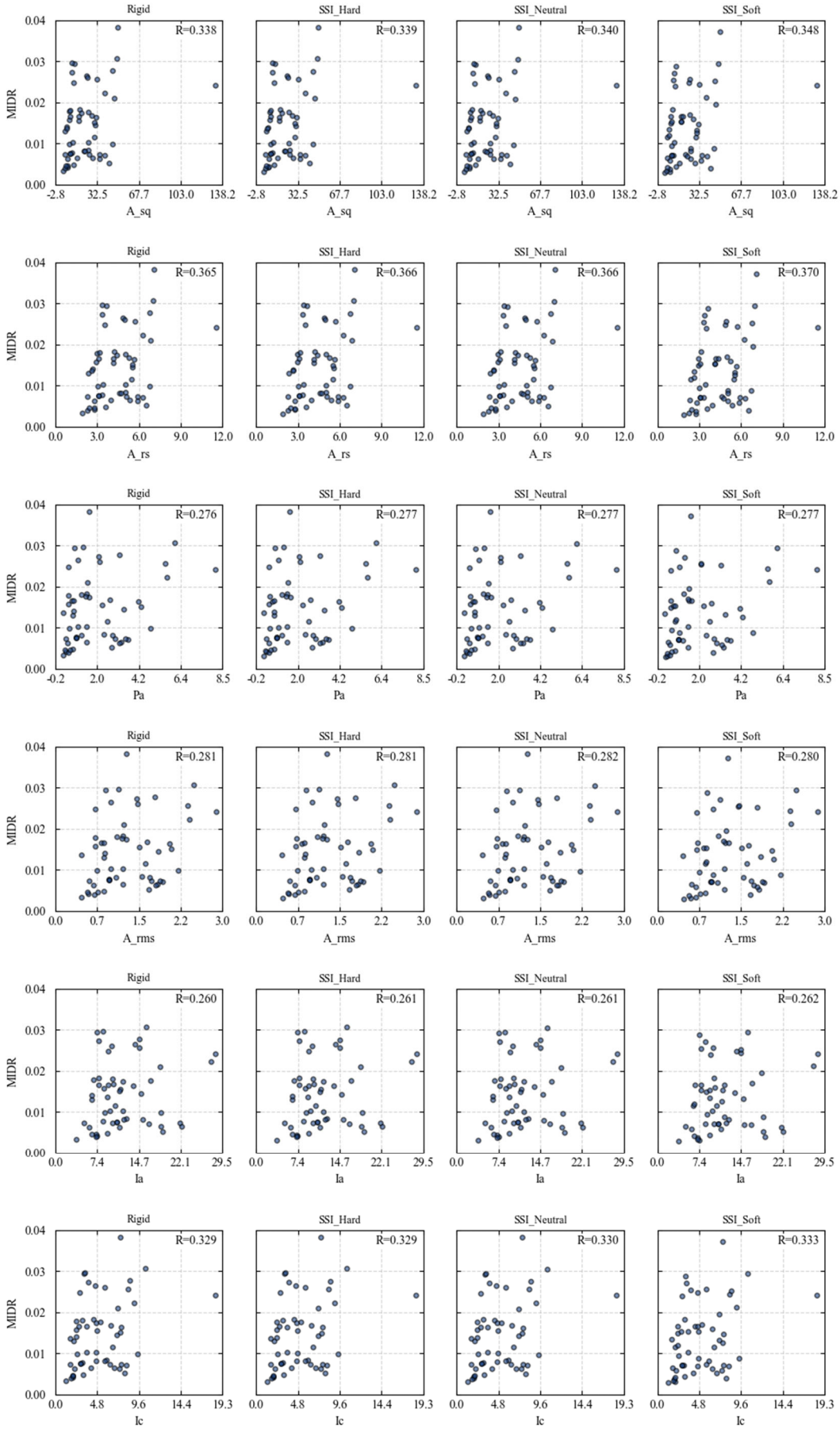


Figure 6. *Cont*.

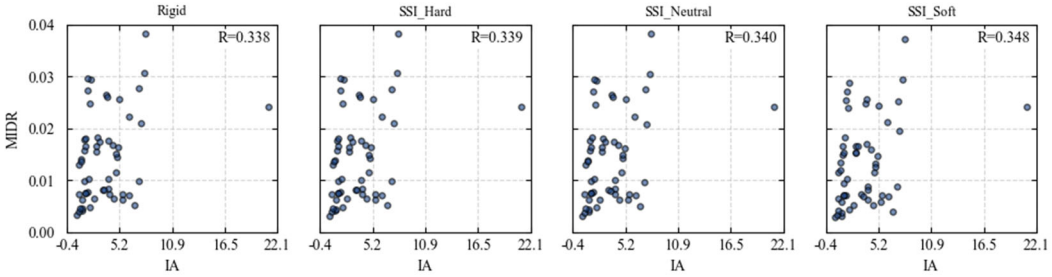


Figure 6. Scatter plots of acceleration-based IMs against MIDR under near-fault ground motions.

Overall, acceleration-based IMs generally show weak correlations with long-period structural responses, regardless of ground motion type. This is mainly due to spectral mismatch between acceleration-based measures and displacement-based demand in long-period systems, as well as the inability of instantaneous or partially averaged acceleration measures to capture the non-stationary characteristics of seismic excitations. Energy-related IMs provide better performance because they incorporate cumulative motion characteristics that are more consistent with structural demand evolution.

3.3.2. Velocity-Based Intensity Measures

Figure 7 presents scatter plots of velocity-based intensity measures versus MIDR for four structural models under far-field ground motions. The Pearson correlation coefficient (R) is reported in each subplot (see figure captions). Under far-field motions, all velocity-based IMs, with the exception of PD, including IF, v_{rs}, PGV, v_{sq}, I_v, Pv, v_{rms}, and SI, systematically exhibit higher correlations with MIDR than acceleration-based measures. This observation is consistent with previous studies showing that velocity-type parameters, such as PGV, perform better in predicting the response of medium- to long-period structures. This further confirms that, for the long-period structure considered herein, displacement demand is primarily governed by the velocity component of ground motion.

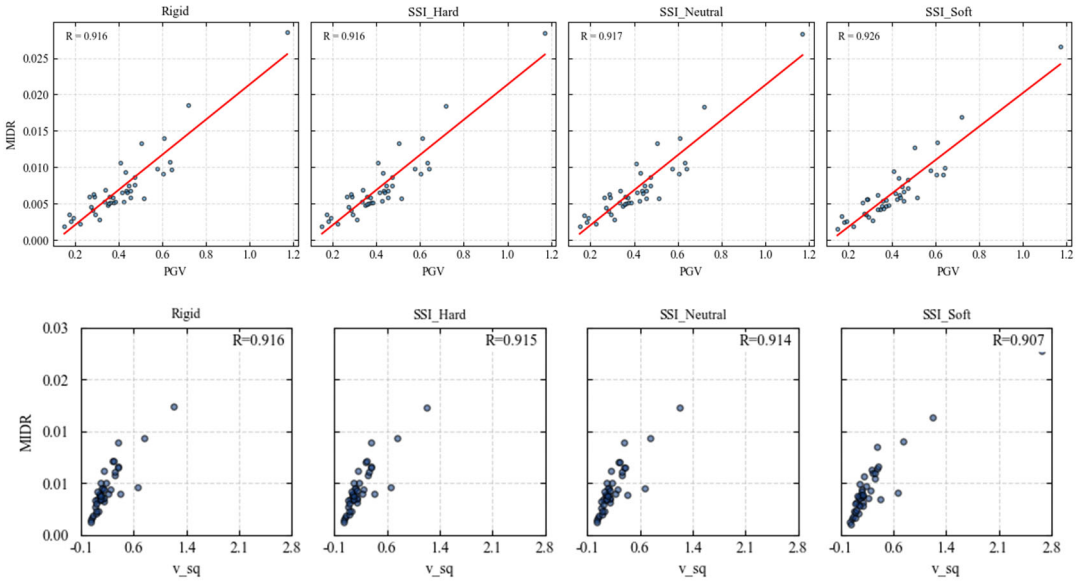


Figure 7. *Cont.*

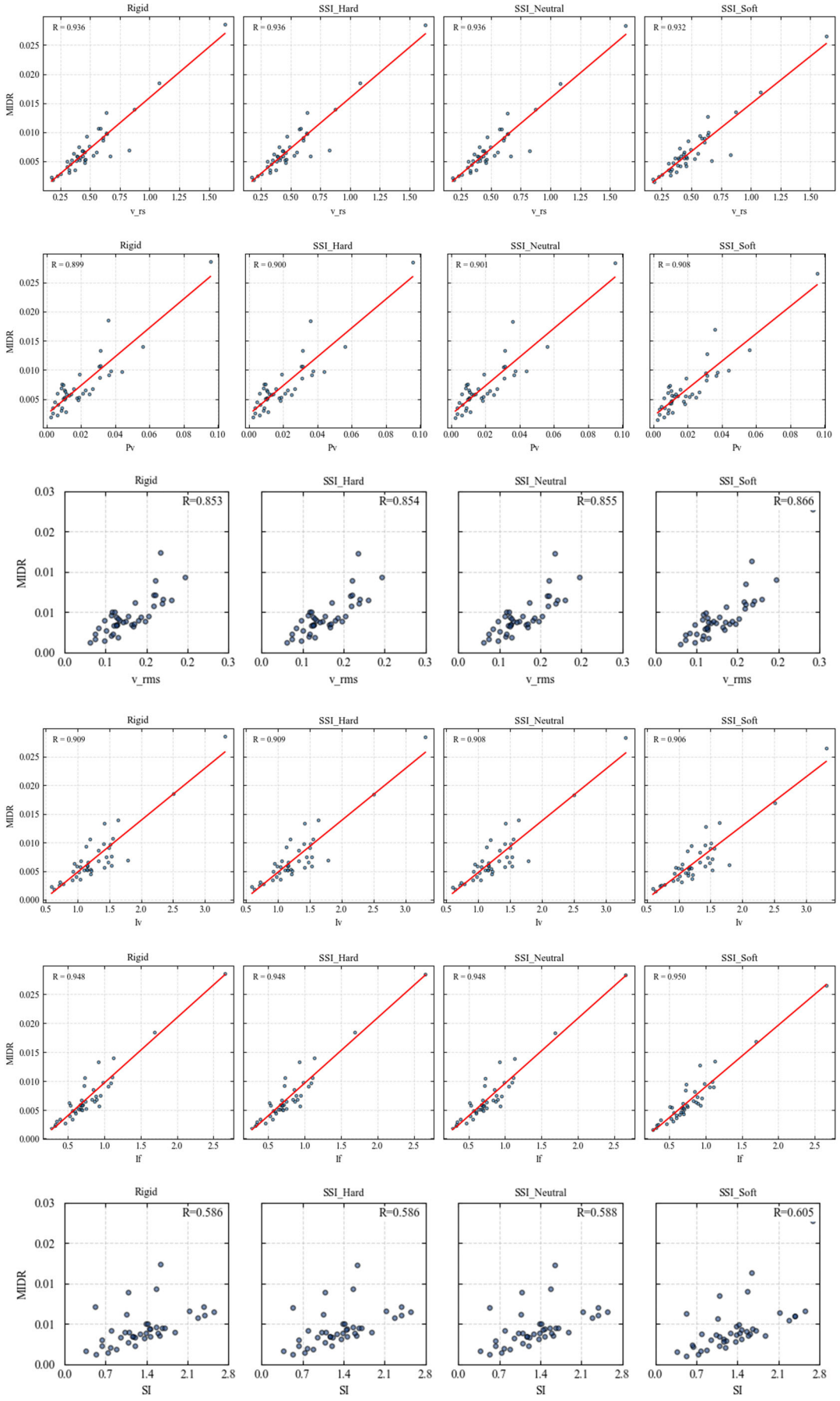


Figure 7. *Cont.*

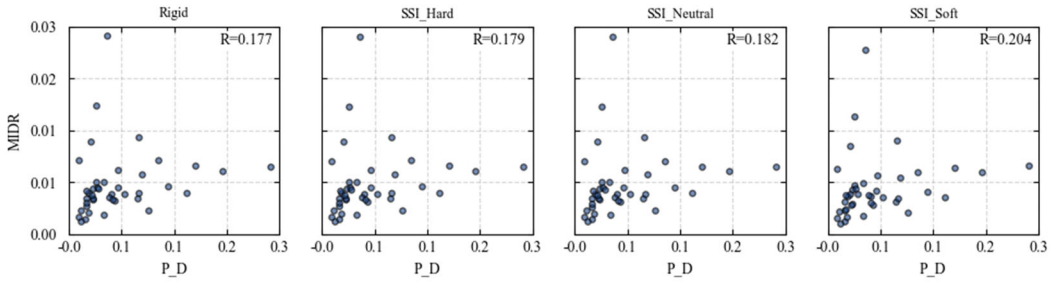


Figure 7. Scatter plots of velocity-based IMs against MIDR under far-field ground motions.

A key finding is that global energy-based velocity measures (e.g., v_{sq} and v_{rs}) exhibit higher correlations with MIDR than local average-based parameters (e.g., Pv and v_{rms}). This behavior is attributed to the energy distribution characteristics of far-field motions, which typically exhibit longer durations and a more gradual energy release process. The nonlinear structural response is therefore governed by cumulative energy accumulation over multiple loading cycles. As a result, global measures representing total input energy are more strongly correlated with peak displacement than local time-window-based measures.

In addition, for velocity-based intensity measures that show relatively strong linear relationships with structural response—such as IF, Iv, PGV, Pv, and v_rs—linear regression trend lines were fitted in the scatter plots to further illustrate their predictive capability. These fitted trends visually confirm the approximate linear dependence between these IMs and MIDR, particularly for PGV and energy-related velocity parameters, reinforcing their suitability as effective predictors of seismic demand.

The correlation between SI and MIDR remains relatively low under far-field motions, primarily due to a period mismatch. SI is defined as the integral of the pseudo-relative velocity spectrum over 0.1–2.5 s, whereas the studied structure has a fundamental period exceeding 3 s, which further increases when SSI effects are considered. Consequently, SI does not fully capture the dominant frequency range of the structural response, thereby limiting its predictive capability. However, the correlation between SI and MIDR increases as soil conditions transition from dense to soft soil. Since the fundamental period of the structure exceeds the upper bound of the conventional SI integration range, the relatively low correlation of SI is mainly attributed to period-range mismatch. The slight change in SI correlation under different soil conditions may reflect indirect record-to-record covariance between short-to-medium-period spectral energy and long-period demand, rather than a direct period-matching effect.

Figure 8 presents scatter plots of velocity-based IMs versus MIDR for four structural models under near-fault ground motions. The Pearson correlation coefficient (R) is shown in each subplot (see figure captions). The fault mechanism significantly affects both the magnitude and ranking of correlations between velocity-based IMs and structural responses.

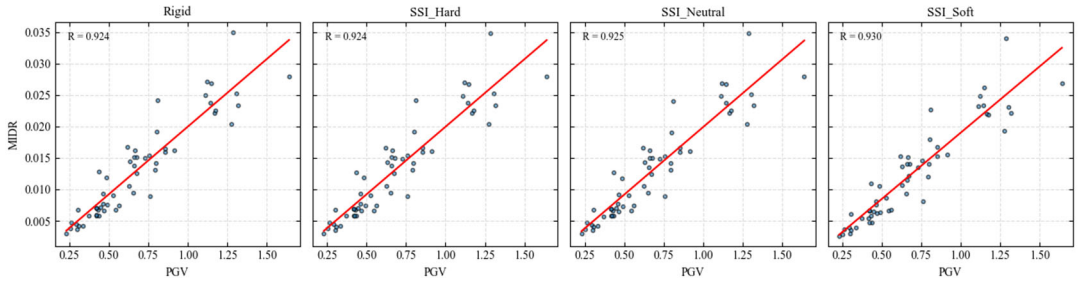


Figure 8. *Cont.*

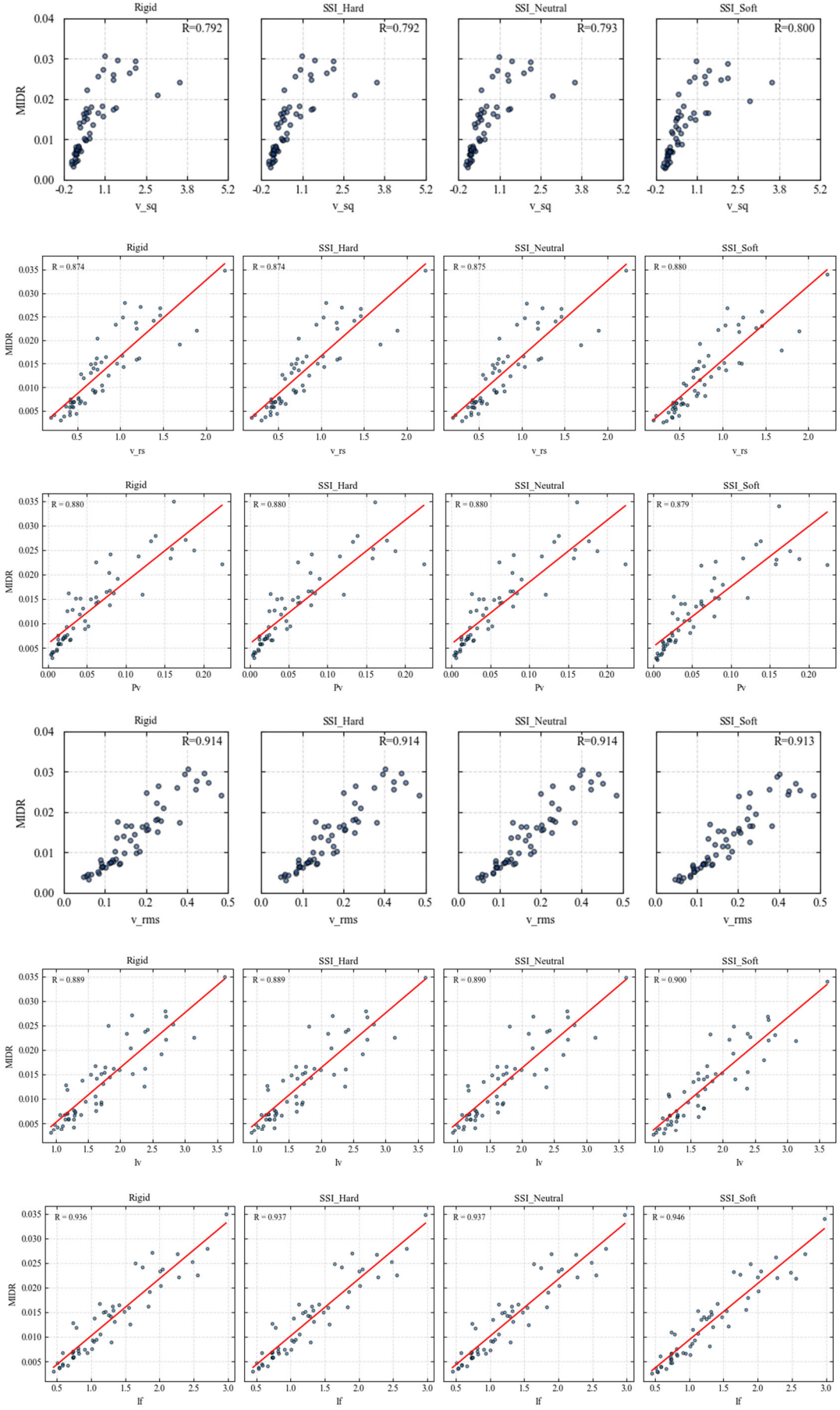


Figure 8. *Cont*.

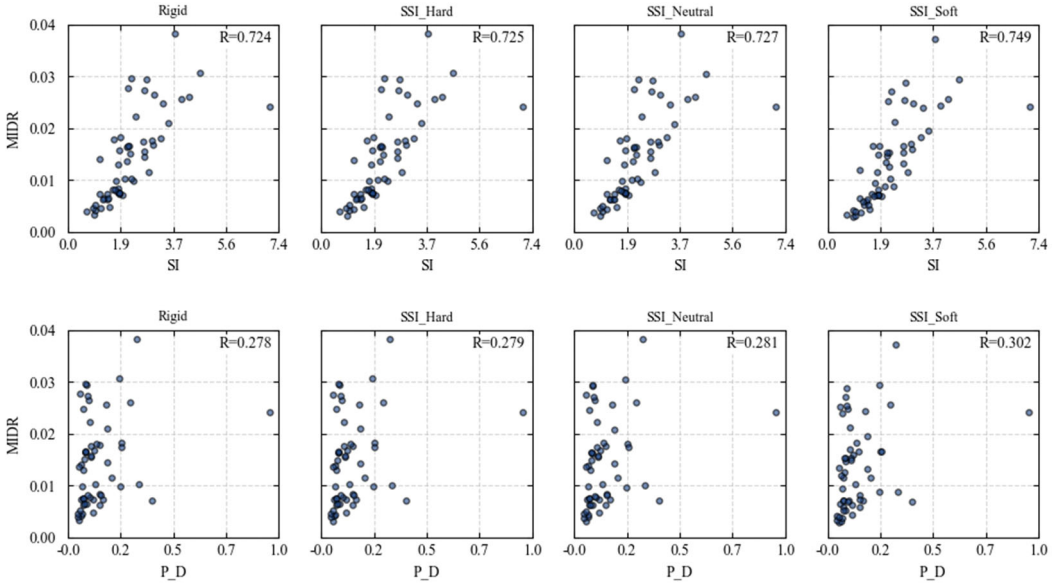


Figure 8. Scatter plots of velocity-based IMs against MIDR under near-fault ground motions.

A key finding is that, compared with far-field motions, the correlation ranking is significantly altered: local average-based parameters (e.g., P_v and v_{rms}) exhibit higher correlations with MIDR than global energy-based parameters (e.g., v_{sq} and v_{rs}). This behavior is primarily attributed to the distinct energy concentration and damage mechanisms of near-fault ground motions. Some near-fault records may contain high-amplitude velocity pulses or concentrated energy release, in which energy is concentrated within a short duration. The structural peak response is therefore governed by a few dominant pulse cycles. In this case, local average-based parameters better capture the effective pulse intensity, whereas global energy-based measures include non-critical post-pulse energy, thereby reducing their correlation with peak response.

In summary, although velocity-based IMs generally perform better for long-period structures, their optimal form depends strongly on the ground motion mechanism. For near-fault motions, local intensity measures are more effective, providing a refined basis for IM selection in performance-based seismic design. The correlation between *SI* and MIDR remains low, consistent with the far-field case, due to the same period-mismatch issue. A slight increase in SI correlation is observed under softer soil conditions, likely due to SSI-induced period elongation and increased energy contributions in lower-frequency ranges.

3.3.3. Displacement-Based Intensity Measures

Figure 9 presents scatter plots of displacement-based intensity measures versus MIDR for four structural models under far-field ground motions. The Pearson correlation coefficient (R) is reported in each subplot (see figure captions). Under far-field motions, the ranking of correlation magnitude between displacement-based IMs and MIDR is clearly influenced by soil conditions. For soft soil sites, the ranking is: PGD > I_d > d_{sq} > d_{rs} > P_d > d_{rms}. For neutral soil conditions, the hierarchy slightly shifts to: I_d > PGD > d_{sq} > d_{rs} > P_d > d_{rms}.

A notable trend is that the correlation between PGD and structural response increases progressively as soil becomes softer, indicating its enhanced sensitivity to foundation compliance under far-field excitations. In contrast, d_{sq} exhibits a decreasing trend with increasing soil softness, suggesting reduced effectiveness in capturing displacement demand under highly deformable soil conditions. Although P_d and d_{rms} show moderate improvement under softer soil conditions, Id demonstrates a reduction in correlation with MIDR as soil flexibility increases. These results highlight that, even under far-field condi-

tions, displacement-based IMs exhibit pronounced soil dependency, reflecting the influence of SSI in modifying the relative contributions of peak and accumulated displacement-related quantities.

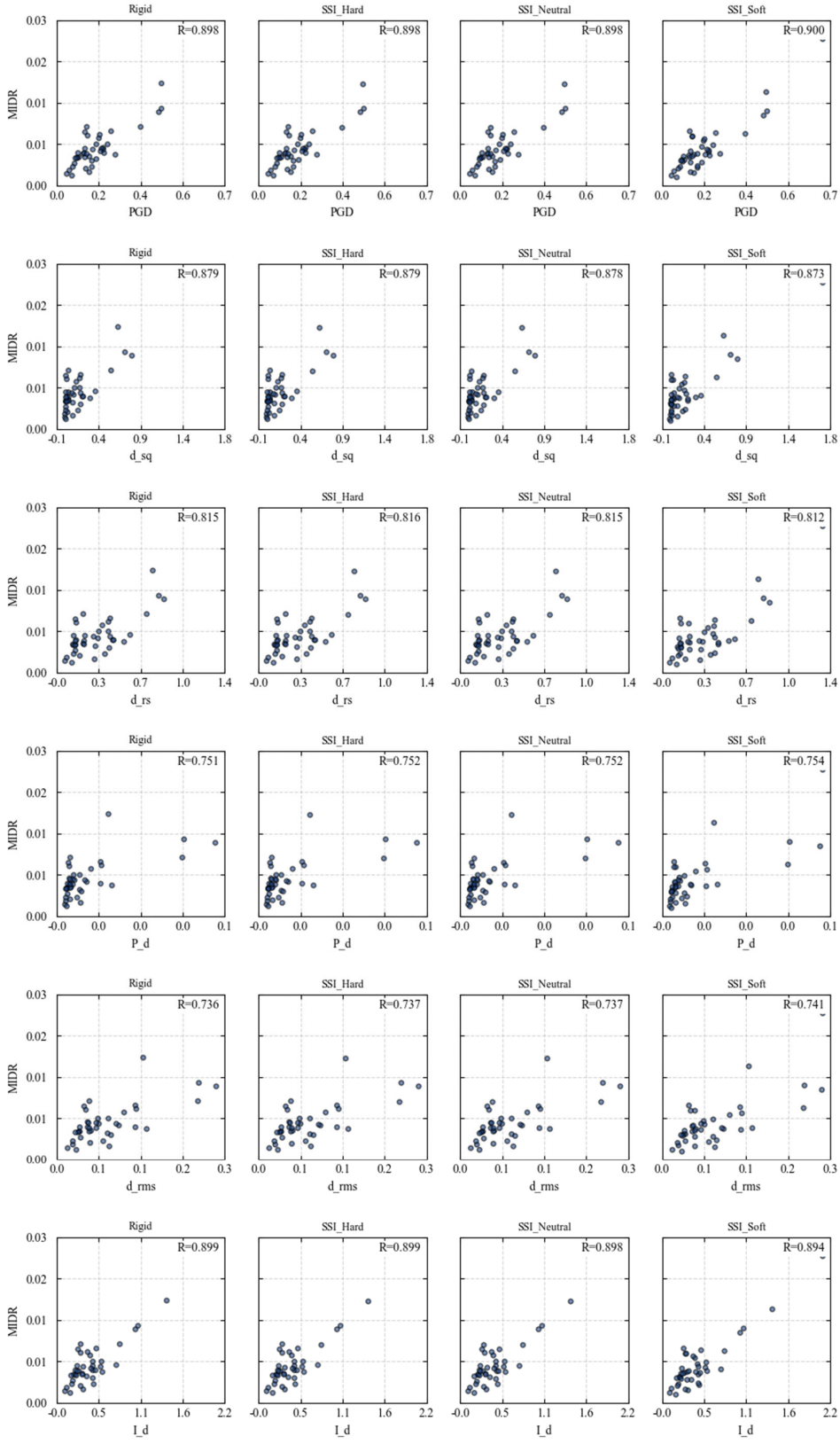


Figure 9. Scatter plots of displacement-based IMs against MIDR under far-field ground motions.

Figure 10 presents scatter plots of displacement-based intensity measures versus MIDR for four structural models under near-fault ground motions. The Pearson correlation coefficient (R) is reported in each subplot (see figure captions). Compared with far-field ground motions (Figure 9), near-fault motions exhibit markedly different soil-dependent correlation patterns for displacement-based IMs. Under near-fault motions, the correlation structure is significantly altered, reflecting the strong influence of pulse-like characteristics and energy concentration effects.

For soft soil sites, the ranking becomes: $PGD > I_d > d_{rms} > d_{rs} > P_d >$ dsq, whereas for the remaining soil conditions, it shifts to: PGD > $d_{rms} > I_d > d_{rs} > P_d > d_{sq}$. In contrast to the far-field case, the correlation between PGD and MIDR decreases progressively with soil softening, indicating that foundation compliance under pulse-like excitation does not necessarily enhance its predictive capability. Similarly, most displacement-based parameters—including d_{sq}, d_{rs}, P_d, and d_{rms}—exhibit an overall decreasing trend with increasing soil softness. This behavior is particularly pronounced for d_{rms}, whose sensitivity to soil compliance is opposite to that observed under far-field motions. Consistent with the far-field results, I_d also shows a reduction in correlation as soil flexibility increases.

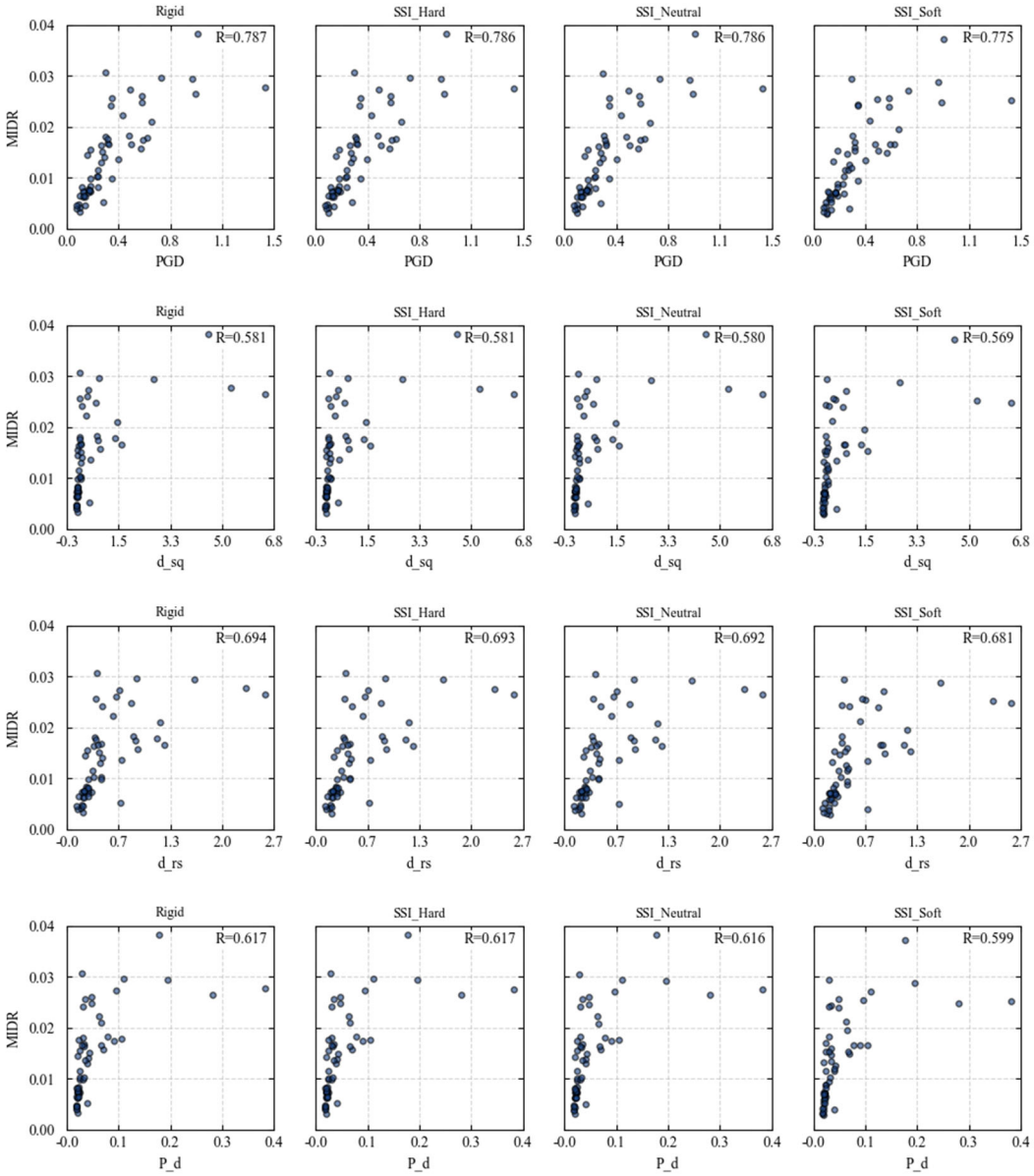


Figure 10. *Cont.*

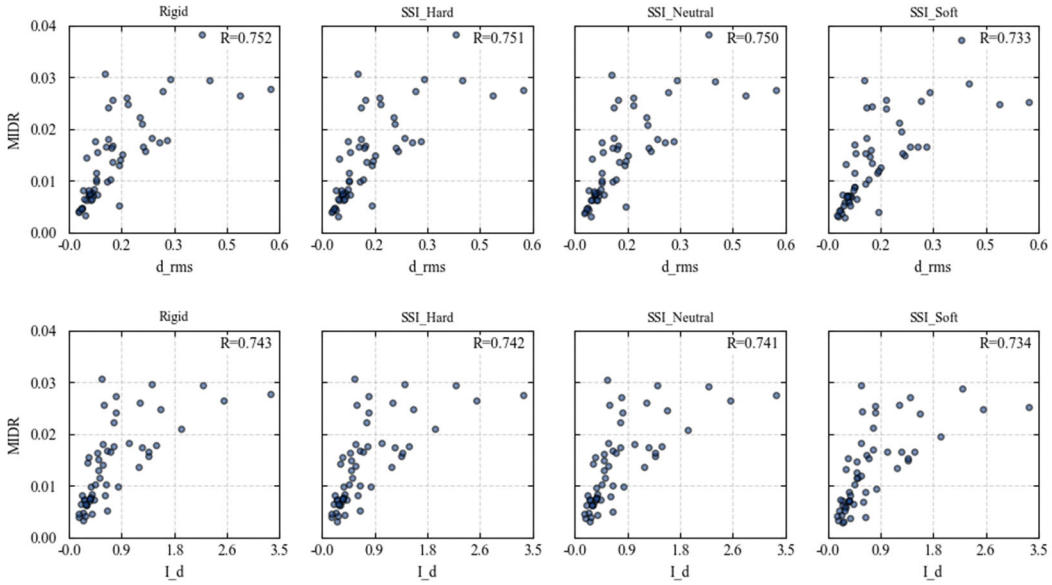


Figure 10. Scatter plots of displacement-based IMs against MIDR under near-fault ground motions.

Overall, these results suggest that near-fault ground motions may alter the soil-dependent correlation patterns of displacement-based IMs, especially when pulse-like components or concentrated long-period energy are present. Under such conditions, SSI effects may interact with near-fault ground motion characteristics, causing peak- and energy-related displacement measures to exhibit different correlation trends from those observed under far-field motions.

4. Conclusions

Based on a comprehensive correlation analysis between ground motion parameters and structural responses, with explicit consideration of SSI effects, the following principal conclusions are drawn, categorized by IM type:

(1) Acceleration-based IMs: The relative correlations of acceleration-based IMs with displacement demand remain largely unaffected by the inclusion of SSI effects. However, for the long-period structure investigated herein, their absolute correlation with MIDR is generally low. This finding confirms the inherent spectral mismatch of acceleration-dominated parameters for such systems. Although SSI further elongates the fundamental period of the structure, it does not mitigate this fundamental limitation.

(2) Velocity-based IMs: Velocity-based IMs generally exhibited higher correlations with MIDR than acceleration-based IMs for the long-period structure investigated in this study, indicating that velocity-related ground motion characteristics are more closely associated with displacement demand under the considered SSI conditions. Nevertheless, the relative correlation performance of velocity-based IMs is influenced by the combined effects of SSI and ground motion type. Under far-field motions, global energy-accumulation parameters (e.g., v_{sq} and v_{rs}) exhibit higher correlations, as SSI often accentuates cumulative damage mechanisms. Under near-fault pulse-type motions, local average-intensity parameters (e.g., P_v, v_{rms}) become highly effective, because the flexible foundation interacts with the concentrated pulse energy. Moreover, the performance of specific parameters such as SI is highly sensitive to period-range mismatch, a limitation significantly exacerbated by SSI-induced period elongation.

(3) Displacement-based IMs: The correlation patterns of displacement-based parameters are most significantly affected by the combined effect of SSI and ground motion type. Notably, the influence of varying soil conditions (a primary driver of SSI) on these

correlations differs fundamentally between far-field and near-fault scenarios. For instance, the correlation of PGD with structural response increases with softer soil under far-field motions but decreases under near-fault motions. This reversal highlights that the influence of SSI is not universal; rather, it is coupled with the frequency content and energy distribution of the input ground motion.

In summary, SSI modifies the IM–EDP correlation patterns in an IM-dependent manner. Its influence is relatively limited for acceleration-based IM rankings and for many velocity-based IMs, but becomes more evident for displacement-based IMs, particularly under soft-soil and near-fault ground motion conditions. The effect of SSI is therefore not merely a uniform scaling of response amplitude; rather, foundation flexibility may act as a dynamic filter that changes the relative importance of different ground motion features, such as cumulative energy and peak instantaneous intensity, depending on both the soil profile and the ground motion type. Accordingly, the results suggest that SSI effects should be considered when interpreting IM–EDP correlations and when screening candidate IMs for performance-based seismic assessment, especially for long-period structures supported by flexible soil profiles. This recommendation should be understood within the scope of the linear-elastic lumped-parameter SSI model adopted in this study.

Author Contributions: Conceptualization, P.L. and J.Y.; methodology, B.Z. and P.L.; writing— original draft preparation, P.L. and B.Z.; writing—review and editing, J.Y. and B.Z. All authors have read and agreed to the published version of the manuscript.

Funding: This research was funded by the Fundamental Research Funds for the Central Universities and grant number (22120230311).

Data Availability Statement: The data presented in this study are available on request from the corresponding author.

Acknowledgments: This study was supported by the Fundamental Research Funds for the Central Universities (22120230311).

Conflicts of Interest: The authors declare no conflict of interest.

References

1. Bojórquez, E.; Chávez, R.; Reyes-Salazar, A.; Ruiz, S.E.; Bojórquez, J. A new ground motion intensity measure IB. *Soil Dyn. Earthq. Eng.* **2017**, *99*, 97–107. [CrossRef]
2. Chen, G.; Yang, J.; Liu, Y.; Kitahara, T.; Beer, M. An energy-frequency parameter for earthquake ground motion intensity measure. *Earthq. Eng. Struct. Dyn.* **2023**, *52*, 271–284. [CrossRef]
3. Hui, S.; Tang, L.; Zhang, X.; Wang, Y.; Ling, X.; Xu, B. An investigation of the influence of near-fault ground motion parameters on the pile's response in liquefiable soil. *Earthq. Eng. Eng. Vib.* **2018**, *17*, 729–745. [CrossRef]
4. Kamal, M.; Inel, M. Correlation between Ground Motion Parameters and Displacement Demands of Mid-Rise RC Buildings on Soft Soils Considering Soil-Structure-Interaction. *Buildings* **2021**, *11*, 125. [CrossRef]
5. Chen, Z.; Wei, J. Correlation between ground motion parameters and lining damage indices for mountain tunnels. *Nat. Hazards* **2013**, *65*, 1683–1702. [CrossRef]
6. Chebihi, A.; Dorbani, S.; Laouami, N. Correlation Between Ground Motion Parameters and Structural Response of Reinforced Concrete Buildings. *Arab. J. Sci. Eng.* **2024**, *49*, 4905–4927. [CrossRef]
7. Li, B.; Lai, Q.; Guo, E.; Mao, C.; Li, X. Determining the Optimal Scalar Intensity Measure of Floor Communication Towers. *Shock Vib.* **2022**, *2022*, 6347334. [CrossRef]
8. Seyedi, D.M.; Gehl, P.; Douglas, J.; Davenne, L.; Mezher, N.; Ghavamian, S. Development of seismic fragility surfaces for re-inforced concrete buildings by means of nonlinear time-history analysis. *Earthq. Eng. Struct. Dyn.* **2010**, *39*, 91–108. [CrossRef]
9. Singh, C.; Choudhury, T. Influence of ground motion variables on the nonlinear seismic demand of masonry-infilled reinforced concrete frames. *Bull. Earthq. Eng.* **2024**, *22*, 4357–4375. [CrossRef]
10. Shi, C.; Du, Y. Effect of ground motion characteristics on the progressive collapse performance of isolated structures. *J. Build. Eng.* **2025**, *112*, 113858. [CrossRef]

11. Durucan, C.; Gümüş, M. Direct use of peak ground motion parameters for the estimation of inelastic displacement ratio of SDOF systems subjected to repeated far fault ground motions. *Earthq. Eng. Eng. Vib.* **2018**, *17*, 771–785. [CrossRef]
12. Wani, F.M.; Vemuri, J. Exploring the association of ground motion intensity measures and demand parameters with ANN-based predictive modeling and uncertainty analysis. *Nat. Hazards* **2025**, *121*, 8849–8898. [CrossRef]
13. Mollaioli, F.; Lucchini, A.; Cheng, Y.; Monti, G. Intensity measures for the seismic response prediction of base-isolated buildings. *Bull. Earthq. Eng.* **2013**, *11*, 1841–1866. [CrossRef]
14. Yang, D.; Pan, J.; Li, G. Non-structure-specific intensity measure parameters and characteristic period of near-fault ground motions. *Earthq. Eng. Struct. Dyn.* **2009**, *38*, 1257–1280. [CrossRef]
15. Wei, B.; Yuan, S.; Lu, A.; Zhang, R.; Yang, Z.; Jiang, L. The contribution of near-fault ground motion velocity pulse to the seismic response of high-speed railway bridge-track system. *Soil Dyn. Earthq. Eng.* **2025**, *198*, 109563. [CrossRef]
16. Wang, X.; Shafieezadeh, A.; Ye, A. Optimal intensity measures for probabilistic seismic demand modeling of extended pile-shaft-supported bridges in liquefied and laterally spreading ground. *Bull. Earthq. Eng.* **2018**, *16*, 229–257. [CrossRef]
17. Athanasopoulos-Zekkos, A.; Saadi, M. Ground Motion Selection for Liquefaction Evaluation Analysis of Earthen Levees. *Earthq. Spectra* **2012**, *28*, 1331–1351. [CrossRef]
18. Zhang, J.; Chen, S.; Wang, T.; Wu, F. Study on correlation between ground motion parameters and soil slope seismic response. *Bull. Eng. Geol. Environ.* **2022**, *81*, 226. [CrossRef]
19. Tao, D.; Ma, Q.; Li, S.; Xie, Z.; Lin, D.; Li, S. Support Vector Regression for the Relationships between Ground Motion Param-eters and Macroseismic Intensity in the Sichuan–Yunnan Region. *Appl. Sci.* **2020**, *10*, 3086. [CrossRef]
20. Wang, X.-C.; Su, W.; Wang, J.-T.; Xu, Y.-J. Engineering evaluation of deterministic ground-motion simulation based on the dynamic response of Pine Flat dam. *Structures* **2025**, *80*, 109667. [CrossRef]
21. Munjy, H.; Habchi, R.; Zareian, F. Validation of Simulated Earthquake Ground Motions for Displacement Response of Building and Bridge Structures Based on Intensity and Frequency Content Parameters. *J. Struct. Eng.* **2022**, *148*, 04021240. [CrossRef]
22. Wang, J.; Xie, Y.; Guo, T.; Du, Z. Predicting the Influence of Soil–Structure Interaction on Seismic Responses of Reinforced Concrete Frame Buildings Using Convolutional Neural Network. *Buildings* **2023**, *13*, 564. [CrossRef]
23. Tuhta, S.; Koç, V.; Günday, F. Effect of Temperature Changes on the Experimental Modal Analysis of a Galvanized Steel Benchmark Structure. *Buildings* **2026**, *16*, 1069. [CrossRef]
24. Günday, F. Structural Health Monitoring of Steel Garage Model with Stochastic Subspace Identification–Covariance Variance Analysis. *Buildings* **2025**, *15*, 944. [CrossRef]
25. Tuhta, S.; Günday, F. Investigation of Steel Chimney Retrofitted with Nanocoating Under Earthquake Excitation Using FEM. *Coatings* **2025**, *15*, 619. [CrossRef]
26. Yang, D.; Chen, H.; Meng, Z.; Chen, G. Random Vibration and Dynamic Reliability Analyses for Nonlinear MDOF Systems under Additive Excitations via DPIM. *J. Eng. Mech.* **2021**, *147*, 04021117. [CrossRef]
27. Etedali, S.; Akbari, M.; Seifi, M. MOCS-based optimum design of TMD and FTMD for tall buildings under near-field earthquakes including SSI effects. *Soil Dyn. Earthq. Eng.* **2019**, *119*, 36–50. [CrossRef]
28. Ma, F.; Zhang, H.; Bockstedte, A.; Foliente, G.C.; Paevere, P. Parameter Analysis of the Differential Model of Hysteresis. *J. Appl. Mech.* **2004**, *71*, 342–349. [CrossRef]
29. Kircher, C.; Deierlein, G.; Hooper, J.; Krawinkler, H.; Mahin, S.; Shing, B.; Wallace, J. *Evaluation of the FEMA P-695 Methodology for Quantification of Building Seismic Performance Factors*; National Institute of Standards and Technology: Gaithersburg, MD, USA, 2010.

Disclaimer/Publisher's Note: The statements, opinions and data contained in all publications are solely those of the individual author(s) and contributor(s) and not of MDPI and/or the editor(s). MDPI and/or the editor(s) disclaim responsibility for any injury to people or property resulting from any ideas, methods, instructions or products referred to in the content.